

Magnetic field simulation and analysis of superconducting magnetic separator with different magnetic matrices

Mingliang Zhou ¹, Lixia Li ¹, Xuebin Su ², Zhe Liu ¹, Feifei Liu ¹, Zhitao Yuan ¹, Jiongtian Liu ³

¹ School of Resources and Civil Engineering, Northeastern University, Shenyang 110819, China

² China National Uranium Company Limited, Beijing 100013, China

³ School of Chemical Engineering, Zhengzhou University, Zhengzhou 450001, China

Corresponding author: lilixia@mail.neu.edu.cn (Lixia Li), suxuebin1968@163.com (Xuebin Su)

Abstract: Superconducting magnetic separator technology exploits the power of intense magnetic fields to discriminate between magnetic and non-magnetic materials, proving indispensable across various sectors including mining, recycling, and water treatment. This study seeks to elucidate the influence of different magnetic gathering media on the magnetic field distribution within superconducting magnetic separators through comprehensive modeling and simulation. Employing *Infolytica MagNet* software, we simulated the magnetic field distribution in a JS-6-102 pilot-scale superconducting magnetic separator, assessing conditions both without magnetic media and with diverse magnetic matrices, including mesh and rod types. Our simulations reveal that the inclusion of magnetic matrices markedly modifies the magnetic field distribution, leading to enhanced magnetic induction intensity and variations in field uniformity. Specifically, we found that smaller mesh sizes produce a more homogeneous magnetic field, whereas larger rod diameters induce greater magnetic field distortion. These insights are pivotal for optimizing the design and operational efficiency of superconducting magnetic separation systems.

Keywords: magnetic field simulation, superconducting magnetic separator, magnetic matrices

1. Introduction

Superconducting magnetic separator (SMS) technology leverages the distinctive properties of magnetic fields to segregate magnetic materials from non-magnetic ones, playing a pivotal role in diverse industries, including mining, recycling, and water treatment (Fuchino et al., 2013; Gillet and Diot, 1999; Iranmanesh and Hulliger, 2017; Maniotis et al., 2023; Wang et al., 2021; Watson and Peter, 2022). Since its inception in the 1970s, this technology has undergone substantial evolution driven by the need for efficient and environmentally sustainable separation processes. Initial applications encompassed the purification of kaolin clay in the paper-coating industry and the treatment of steel industry wastewater, thereby laying the groundwork for contemporary advanced systems.

During the 1980s, large superconducting magnets were employed in the field coils of high-gradient magnetic separation (HGMS) systems, specifically for kaolin clay purification (Iannicelli et al., 1997; Ohara et al., 2001; Sharma, 2021; Watson, 1994). Subsequent advancements in superconducting materials and refrigeration technologies have further propelled the application of SMS technology. Characterized by high magnetic field intensity, large processing capacity, low energy consumption, and reduced operational costs, SMS technology is poised to revolutionize magnetic separation (Ahoranta et al., 2003; Supreeth et al., 2022; Yamato et al., 2020).

Optimizing the magnetic field within the separation zone is crucial for enhancing the performance of magnetic separators. Numerical simulations have become indispensable for this purpose (Xue et al., 2020; Xu et al., 2021; Zheng et al., 2022). Contemporary research focuses on accurately modeling the magnetic field distribution produced by superconducting magnets. High-fidelity simulations employing finite element methods (FEM) and other numerical techniques provide precise predictions of magnetic field profiles (Cao et al., 2019; Hu et al., 2020; Nakai et al., 2010). Additionally, dynamic

simulations that account for particle movement within the magnetic field are being explored (Liu et al., 2022; Luo and Nguyen, 2017; Wang et al., 2020). These studies are essential for understanding the mechanisms of separation and the efficiency of SMS systems. Furthermore, numerical simulations have been applied to the design of superconducting magnets for vertical-ring high-gradient magnetic separation systems (Zheng et al., 2022).

Recent advancements in magnetic field simulation include the work of Xue et al., who developed a model incorporating particle sets and magnetic matrices of various cross-sectional shapes (round, oval, square, and diamond) to study axial HGMS systems, providing valuable insights into the selection of magnetic matrices for separation (Xue et al., 2022). Zhou et al. investigated the characteristics of induced magnetic fields in elliptical magnetic matrices and explored the effects of structural parameters on magnetic particle adsorption, revealing that interactions in multi-matrix composite systems vary with matrix size and spacing (Zhou et al., 2021). Li et al. demonstrated that spiral-shaped magnetic media more effectively enhance the magnetic field gradient compared to smooth rod matrices, thus improving the recovery of fine-grained iron minerals (Li et al., 2019). Zheng et al. simulated the magnetic field generated by different matrix shapes using ANSYS software, focusing on magnetic field strength, gradient, and magnetic force. Their simulations indicated that diamond-shaped, elliptical, square, and circular steel matrices reach magnetization saturation at approximately 0.7, 0.8, 1.0, and 1.1 T, respectively. The magnetic field gradient increases with magnetic induction until saturation, after which it stabilizes. Elliptical and square matrices exhibited robust magnetic characteristics over a broad induction range. Square matrices produced the highest surface magnetic force, albeit with a rapid decline and limited depth. Conversely, elliptical matrices showed a slower decrease, providing a deeper effect. Diamond-shaped matrices reached saturation quickly, resulting in the fastest reduction in magnetic force.

Despite extensive documentation of magnetic field simulations for weak field separators and high-gradient strong field separators, there remains a notable gap in systematic research focusing on the magnetic field distribution within SMS systems. Unlike conventional separators, SMS technology operates under markedly different conditions, where extreme field strengths and the unique behavior of superconducting materials introduce complex dynamics that are not yet fully understood. This lack of comprehensive research impedes efforts to optimize SMS design and performance, which are increasingly critical for applications requiring highly efficient separation processes. Addressing this gap through detailed simulation and experimental analysis could lead to significant advancements in SMS effectiveness, paving the way for broader industrial adoption and enhanced operational efficiency.

This study aims to investigate the impact of various magnetic gathering media on the magnetic field within SMS machines through precise modeling and simulation. The primary research focuses include the development of an accurate model, the implementation of advanced magnetic field simulation methods, and the analysis of the effects of different magnetic gathering media.

2. Materials and methods

2.1 Equipment

A JS-6-102 pilot-scale superconducting magnetic separator (SMS), developed by Jiangsu Jingkai Zhongke Superconducting High Technology Co., Ltd., China, and depicted in Fig. 1, was selected as the research subject. The equipment's background magnetic field is adjustable within a range of 0-6T, and it features a reciprocating separation tank with a diameter of 102.0 mm. During operation, the reciprocating separation tank is positioned within the superconducting magnet system. Magnetic minerals are adsorbed onto the magnetic media, while non-magnetic minerals are flushed out with the washing water and pulp. After separation, the reciprocating tank is retracted from the separation zone, allowing the washing water to remove the magnetic minerals.

2.2 Simulation software

Infolytica MagNet, a widely recognized magnetic field simulation software, is extensively employed across various industries for the design and optimization of electromagnetic devices, including motors, transformers, actuators, and magnetic separation systems. *MagNet* addresses electromagnetic field

challenges by leveraging Maxwell's equations, the foundational principles governing the behavior of electromagnetic fields, including the distribution of electric and magnetic fields, as well as charge and current distributions. Maxwell's equations fundamentally describe the behavior of electromagnetic fields, encompassing the distribution of electric and magnetic fields, along with the distributions of charges and currents.

MagNet employs the finite element method (FEM) to discretize Maxwell's equations, converting complex electromagnetic field problems into systems of algebraic equations, which are subsequently solved through numerical techniques. Specifically, *MagNet* partitions the spatial domain into a finite number of elements, approximates the electromagnetic field within each element using simple functions, and subsequently formulates the system's algebraic equations based on the interconnections of these elements. Finally, iterative algorithms are employed to resolve these algebraic equations, yielding a precise numerical solution for the electromagnetic field.



Fig. 1. A JS-6-102 pilot-scale superconducting magnetic separator

2.3. Magnetic separation theory

The superconducting magnetic system, depicted in Fig. 2, illustrates that when a gradient magnetic field is applied to a magnetized particle, the magnetic forces exerted on its two poles are asymmetric. Consequently, the particle experiences a net force, inducing its movement and facilitating its separation. This phenomenon underpins the fundamental principle of magnetic separation.

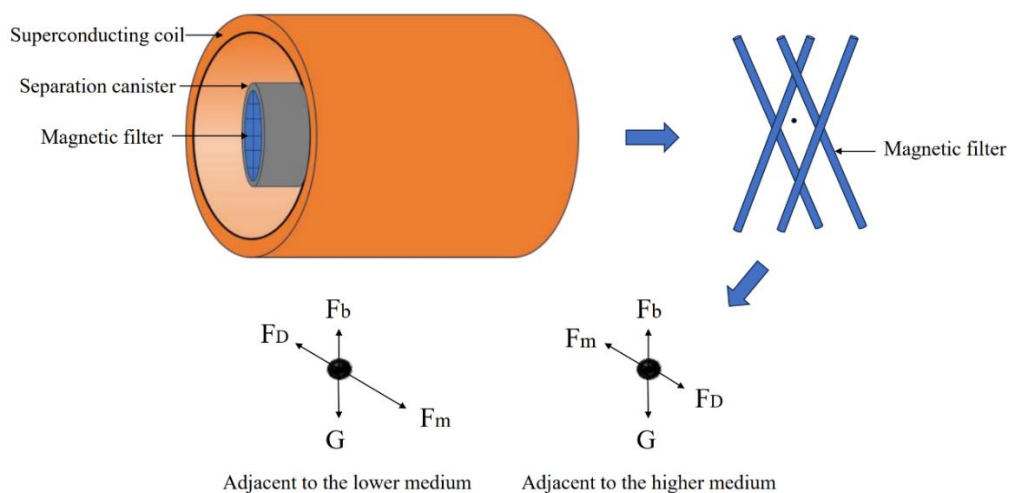


Fig. 2. Magnetic system structure and particle force analysis

The net force experienced by a magnetized particle in a magnetic field is related to the magnetization intensity of the particle, the volume of the particle, the strength of the external magnetic field, and the gradient of the magnetic field. The force can be calculated using the equation below:

$$mH - m \left(H - \frac{dH}{dl} l \right) = ml \frac{dH}{dl} = P_m \frac{dH}{dl} \quad (1)$$

$$P_m = \kappa V H \quad (2)$$

where m is the magnetic pole strength, H is the magnetic field strength, l is the length of the mineral grain in the direction of the magnetic field, dH/dl is the magnetic field gradient, P_m is the magnetic moment. V is the volume of the particle, κ is the magnetic susceptibility of the particle.

The drag force F_D to the particle from the fluid is shown by:

$$F_D = 6\pi\eta r(v_F - v_p) \quad (3)$$

where η , r , v_F and v_p are the fluid viscosity, radius of the spherical particle, fluid velocity and particle velocity, respectively.

The gravity and buoyancy can be calculated by:

$$G = \frac{4}{3}\pi r^3 \rho_0 g \quad (4)$$

$$F_b = \frac{4}{3}\pi r^3 \rho_1 g \quad (5)$$

where ρ_0 , ρ_1 are particle density and fluid density, respectively.

2.4 Magnetic system modeling

The model constructed for the magnetic system of the Jiangsu Jingkai JS-6-102 horizontal SMS is illustrated in Fig. 3, where the yellow region denotes the excitation coil. The blue region indicates the magnetic yoke, designed to augment the attraction force of the electromagnetic coil by confining the magnetic field lines within its interior, thereby enhancing the efficiency of the electromagnet. The black region corresponds to the non-magnetic stainless steel separation chamber, while the outermost air boundary delineates the computational domain.

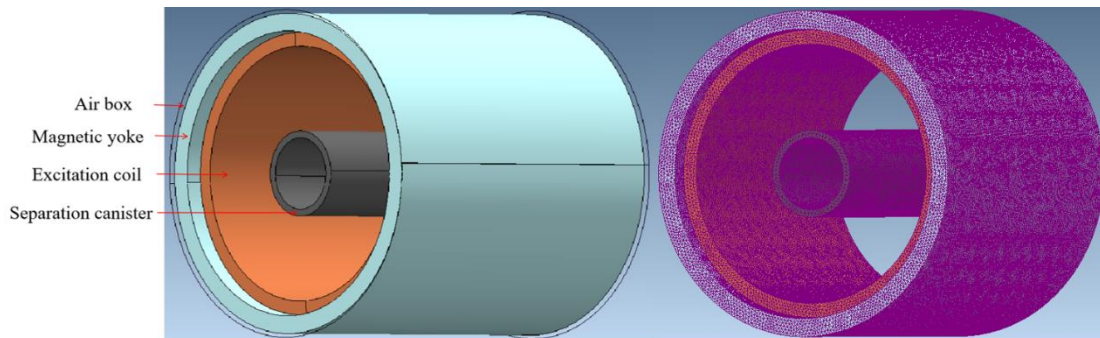


Fig. 3. Modeling of the magnetic system

The SMS is primarily composed of coils and a yoke, with the material composition and winding turns of the coils being critical parameters that dictate the strength and distribution of the magnetic field. For the JS-6-102 superconducting magnetic separator, the coils are made from a copper-based niobium-titanium superconducting alloy. The coils have an inner diameter of 716.4 mm, an outer diameter of 793.2 mm, a thickness of 38.4 mm, and a length of 885.0 mm. Each coil comprises 38 layers with 650 turns per layer, and the operating current is set at 200 A. The yoke is constructed from Mu4 soft magnetic material, characterized by a magnetic permeability of 10,000 H/m.

For the meshing process, tetrahedral structural elements are employed, with the mesh refined in regions of interest to ensure computational accuracy. The maximum mesh size is set at 5.0 mm, and the software performs adaptive analysis until the meshing precision meets the necessary computational criteria.

The Newton-Raphson algorithm, a well-established iterative method for approximating numerical solutions of equations, is employed for simulation calculations. This method is particularly suited for continuously differentiable nonlinear equations. The algorithm iteratively refines an initial guess by computing the derivative of the function to determine the tangent line, with the intersection of this

tangent and the x-axis providing a new approximation for the root. This iterative process continues until the specified accuracy is attained.

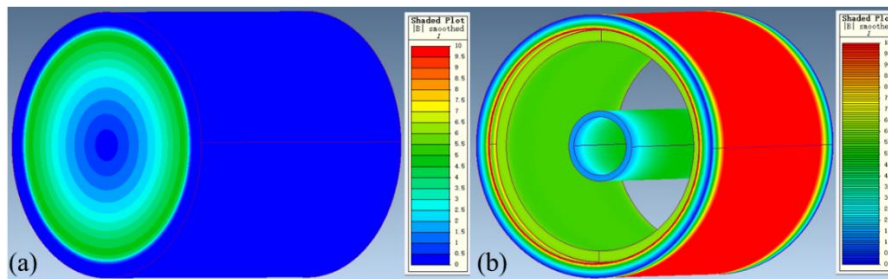
The maximum number of iterations for the Newton-Raphson method is capped at 20, ensuring that if convergence is not achieved within these iterations, the process terminates to prevent excessive computational resource consumption. The Newton tolerance is set at 1%, meaning that the iteration is considered successful once the error falls below this threshold.

Similarly, the conjugate gradient (CG) method's tolerance is set at 0.01%, ensuring that the iterative process is sufficiently close to the solution. If the error at any step is within this tolerance, the iteration is deemed to have converged to the desired solution.

3. Results and discussion

3.1 Simulation without medium

When the separation chamber is devoid of any medium, the magnetic field characteristics are primarily influenced by the external current-induced magnetic field and the chamber's geometric and material properties. The magnetic field distribution within the separation chamber, under conditions where no medium is present, is analyzed, and the corresponding results are presented in Fig. 4.



(a) Cloud map with air box; (b) Cloud map without air box

Fig. 4. Cloud maps of magnetic field distribution in the absence of a medium

Fig. 4(a) presents the cloud map including the air package, demonstrating that the magnetic induction intensity outside the yoke approaches zero, thereby confirming the absence of magnetic leakage. Fig. 4(b) displays the cloud map with the air package concealed. This figure reveals that the magnetic induction intensity is notably stronger around the yoke and coil, while it diminishes inside the separation chamber.

To analyze the magnetic field of the medium-free magnetic system, a cross-sectional view along the XZ+Y plane is selected. The cloud map, contour map, and vector map of the magnetic field distribution on this plane are examined individually, with the results illustrated in Fig. 5.

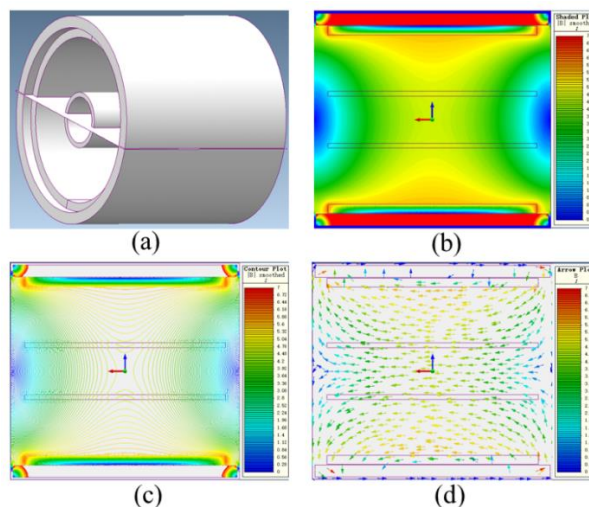


Fig. 5. Analysis of magnetic field characteristics on specific cross-section

The magnetic field distribution cloud map illustrates that within the coil, the field exhibits a distinct dumbbell-shaped profile. Radially, the field strength is elevated near the coil and diminishes with increasing distance. Axially, the field strength peaks at the center and progressively weakens towards both ends, creating broader regions of low magnetic field intensity at the peripheries.

The contour map reveals that the magnetic field contour lines are sparse radially, signifying a relatively low magnetic field gradient. Conversely, axially, the contour lines are sparse at the center of the separation chamber and become progressively denser towards the ends, reflecting an increasing magnetic field gradient.

The vector map of the magnetic field distribution indicates that the magnetic field lines traverse from one end of the separation chamber to the other along an arcuate path, with greater curvature near the axis.

Extract a line segment from the location indicated in Fig.6(a), plot the variation in magnetic induction intensity along this segment, and conduct a fitting analysis. Fig .6(b) illustrates the magnetic field variation within the separation zone of the superconducting magnetic separator in the absence of media.

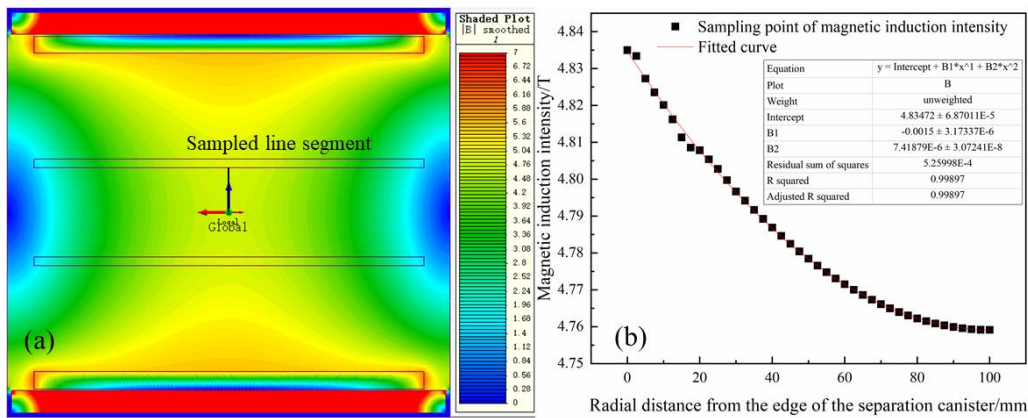


Fig. 6. Magnetic induction intensity fitting of the sampled line segment

The variation of magnetic induction intensity on the intercepted line segment shown in Fig. 6 can be synthesized by the following formula:

$$y = A + B_1x + B_2x^2 \quad (6)$$

where A is $4.83472 \pm 6.87011 \times 10^{-5}$, B₁ is $-0.0015 \pm 3.17337 \times 10^{-6}$, B₂ is $7.41879 \times 10^{-6} \pm 3.07241 \times 10^{-8}$. An R-squared value of 0.99897 indicates that 99.897% of the variance in the dependent variable is explained by the independent variables in the model. This implies an extremely high degree of fit, meaning the model accurately represents the data. The Adjusted R squared value also being 0.99897 means that even after adjusting for the number of predictors in the model, the explanatory power remains very high. Typically, the Adjusted R squared accounts for the number of predictors and penalizes the addition of irrelevant variables. The fact that both values are the same suggests that all predictors in the model contribute significantly to explaining the variance, and the model is not overfitted.

In addition, the variation of the magnetic field gradient along the line can be obtained by calculating the first derivative of this formula.

3.2 Simulation with magnetic matrix

A magnetic matrix is a material characterized by distinct magnetic properties. When subjected to an external magnetic field, its magnetization intensity increases markedly, thereby influencing the surrounding magnetic field. The introduction of a magnetic matrix enhances the magnetic induction strength in its vicinity. When exposed to an external magnetic field, the internal magnetic particles align in a specific direction, thereby intensifying the magnetic induction in the affected region. The magnetic matrix also modifies the distribution of magnetic fields. Due to the unique properties of its internal microstructure, it can guide magnetic field lines to generate specific distribution patterns within or around the matrix, thereby affecting the propagation and utility of magnetic fields.

Magnetic matrices are typically composed of magnetically conductive stainless steel and can be classified into various forms, including spherical, toothed, steel wool, mesh, and rod media. Typically, when the medium's magnetization has not reached saturation, sharper geometrical features and smaller relative sizes result in a higher magnetic field gradient. Using the ferromagnetic matrices depicted in Fig. 7 as the subject of investigation, the study examines the variations in their effects on magnetic induction intensity.

The materials shown in Fig. 7 (a) are mesh media, with side lengths of 0.6mm, 1.0mm, 1.4mm, and 1.8mm respectively, forming rhombuses with side lengths of 2.0mm, 3.0mm, 4.0mm, and 7.0mm. The materials shown in Fig. 7 (b) are rod media, with diameters of 1.0mm, 1.5mm, 2.0mm, and 3.0mm respectively, with adjacent rod spacings of 1.0mm, 1.5mm, 2.0mm, and 3.0mm respectively. The magnetic matrix in this research adopts magnetically conductive stainless steel, and its B-H curve is shown in Fig. 8.

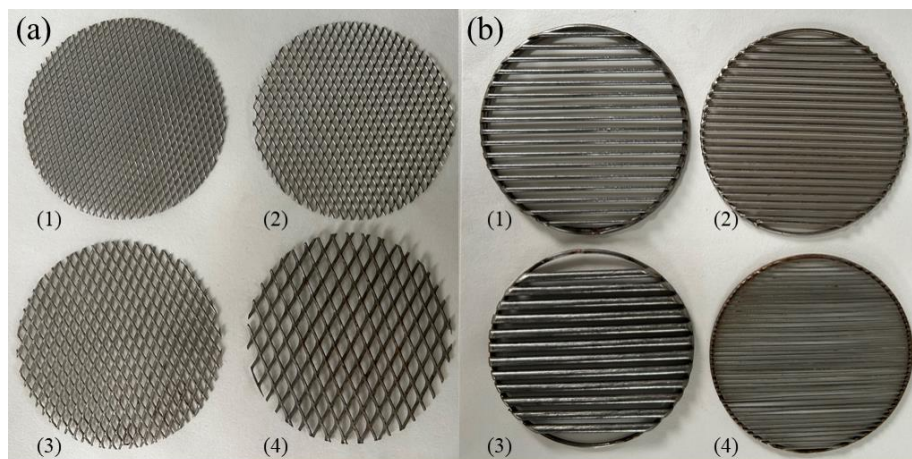


Fig. 7. Magnetic matrix



Fig. 8. B-H curve of magnetic matrix materials

To model the mesh media at a 1:1 scale, but considering that the dimensions of the magnetic system are much larger compared to the diameter of the media, requiring a significantly small grid size for simulation calculations, incorporating the mesh media into the selection area for calculation would consume a tremendous amount of computational resources. Therefore, to demonstrate the effects of different mesh media on the magnetic field, this study reduced the size of the magnetic system while ensuring that its magnetic field intensity remained consistent with the original size for modeling. The results are shown in Fig. 9.

The simulated analysis of the modeled system involves capturing cross-sectional XY planes passing through the axis (as shown in Fig. 10), to compare the effects of different specifications of mesh media on the magnetic field.

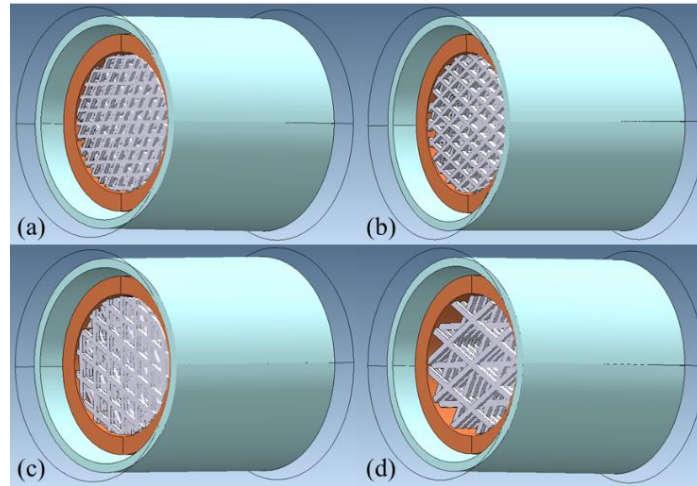


Fig. 9. Modeling of different mesh media

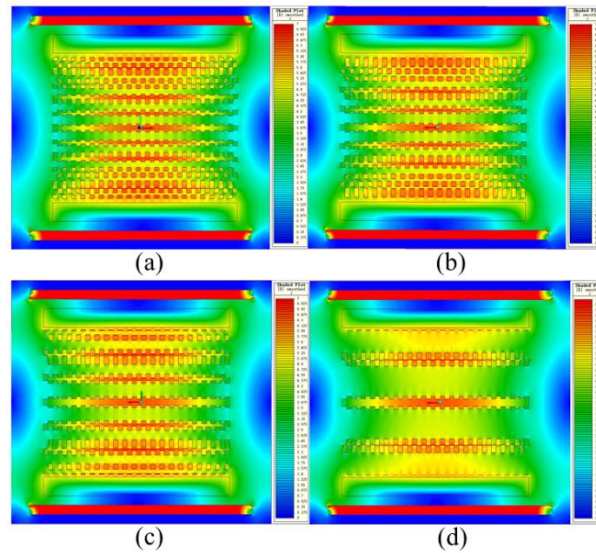


Fig. 10. Magnetic field distribution captured across the axis YZ plane

Referring to the magnetic field distribution simulated for various mesh media as illustrated in Fig. 10, it is observed that regardless of whether the mesh dimensions are 2.0mm×4.0mm, 3.0mm×6.0mm, 4.0mm×8.0mm, or 7.0mm×12.0mm, the magnetic field distribution within the separation zone consistently exhibits a dumbbell shape. The field intensity is elevated near the periphery adjacent to the coil and diminishes toward the center. Along the axial direction, the magnetic field intensity is lower at the extremities and higher at the center. As the gap between the mesh media increases, the magnetic focusing effect diminishes, leading to reduced uniformity in the magnetic field distribution and a more pronounced dumbbell shape. Overall, the magnetic field intensity within ferromagnetic materials surpasses that in the voids of the mesh media. This enhancement is attributed to the high magnetic permeability of ferromagnetic materials, which facilitates the concentration of magnetic field lines within the material. In contrast to water or other low-permeability substances, ferromagnetic materials offer a path with reduced magnetic resistance, thereby channeling the magnetic field through these materials and intensifying the field within them.

The impact of magnetic matrices on the magnetic field within the separator is primarily reflected in variations in the magnetic field gradient. Consequently, Fig. 11 illustrates the distribution of magnetic flux lines for mesh media of various sizes. It is evident that as the mesh size increases, the magnetic flux line distribution in the separation area becomes increasingly non-uniform, with higher density near the magnetic matrices and lower density further away. Conversely, smaller mesh sizes result in a more uniform distribution of magnetic flux lines.

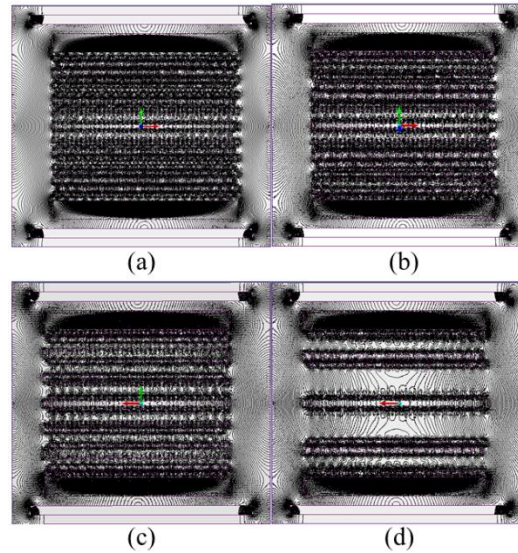


Fig. 11. Differences in the distribution of magnetic inductance lines

The actual separation zone is characterized by a region where the axial magnetic induction intensity is more uniformly distributed within the coil. As illustrated in Fig. 12, the magnetic induction intensity varies with the position where it intersects with the mesh medium near the axis. The superposition of the mesh medium leads to irregular variation in magnetic induction intensity. However, overall, the intensity within the mesh gradually increases with the diagonal size of the mesh medium. Nonetheless, the magnetic field gradient remains relatively low. Decreasing the grid size creates additional pathways for magnetic field lines, thereby enhancing the uniformity of the magnetic field distribution to a certain extent. This effect is attributed to the magnetic field's tendency to propagate along paths with higher magnetic permeability. Smaller grids reduce local magnetic resistance, thus facilitating a more uniform magnetic field distribution within the media.

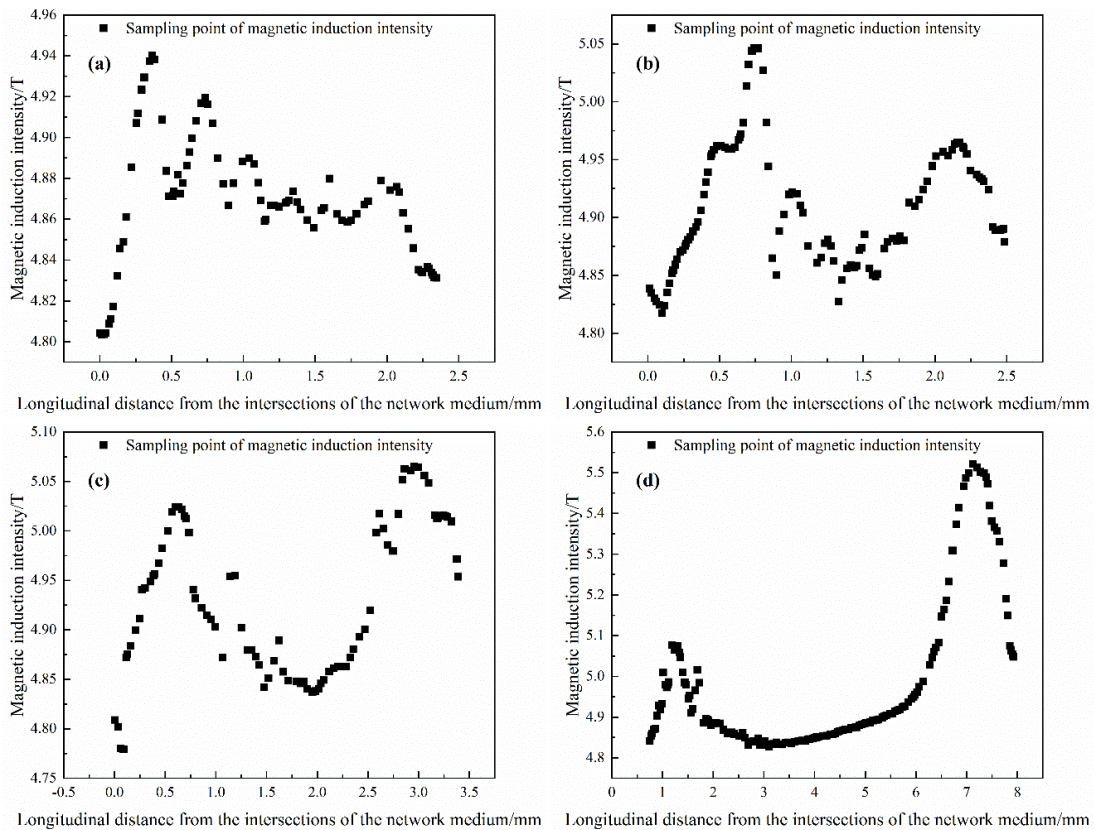


Fig. 12. The magnetic induction intensity on the surface of the polymagnetic matrices varies with distance

Employing a similar methodology, rod media can be analyzed, as illustrated in Fig. 13. The introduction of rod media with varying diameters into a magnetic field influences the magnetic field distribution. The magnetic permeability and geometric dimensions of rod-shaped media, particularly their diameters, significantly impact the direction and density of magnetic field lines. Fig. 14 presents the XY cross-section along the axis, illustrating the effects of rod media with different diameters on the magnetic field, as simulated and analyzed.

The simulation results show that rod media and mesh media exhibit similar magnetic field distributions. When rod-shaped media with different diameters are placed in the same magnetic field, they will have different effects on the magnitude distribution and uniformity of the magnetic field. Around rod media with smaller diameters, the magnetic field distribution may be more uniform because their influence on the magnetic field is weaker, and the bending and focusing effects of magnetic field lines are less pronounced compared to larger-diameter rods. In contrast, larger diameter rod media may create stronger magnetic field distortions and focus around them, which may lead to uneven magnetic field distributions, especially in areas near the media.

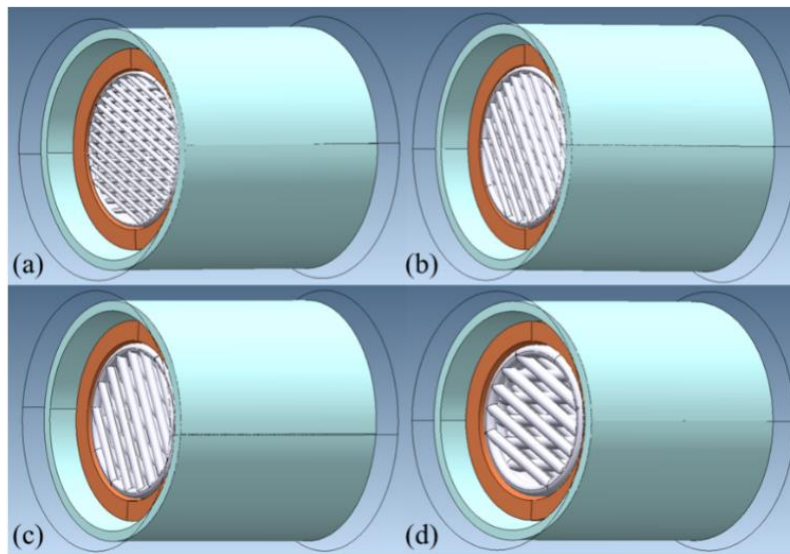


Fig. 13. Modeling of different rod media

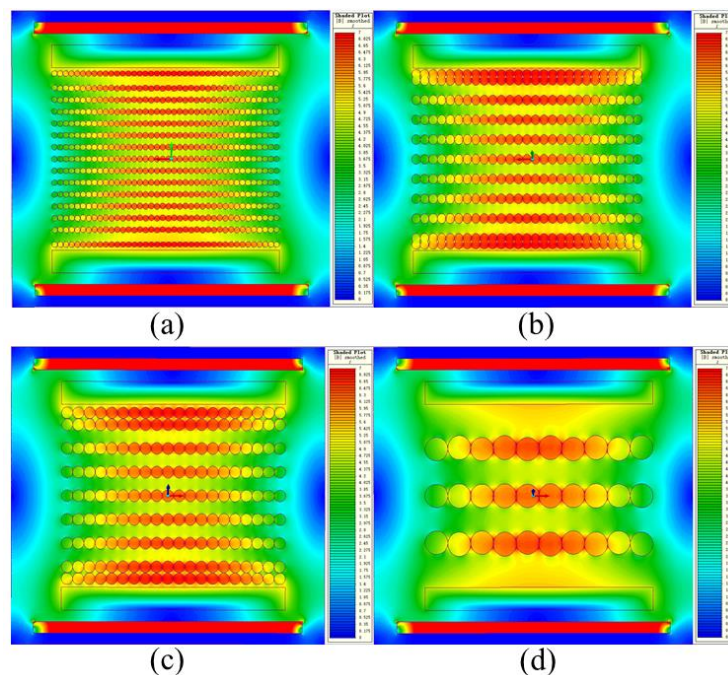


Fig. 14. The magnetic field distribution in the XY cross-section of different rod media

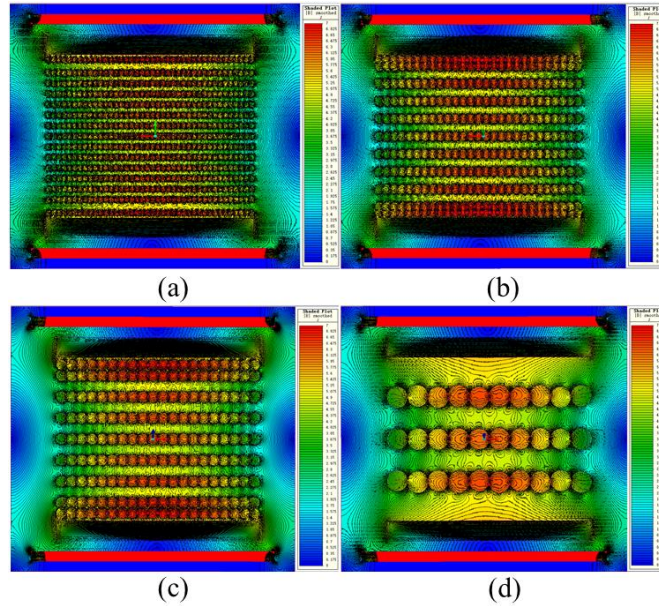


Fig. 15. Differences in the distribution of magnetic inductance lines

The magnetic field lines vary with different diameters of ferromagnetic stainless steel rods. For rods with smaller diameters, the magnetic field lines are denser near the rod's surface. As the diameter of the ferromagnetic rods decreases, the surface area-to-volume ratio increases, resulting in a higher density of magnetic field lines near the surface. Consequently, the magnetic field lines are observed to be denser. A dense distribution of magnetic field lines signifies a substantial variation in magnetic field strength within that region, indicating a pronounced magnetic field gradient. The magnetic field gradient represents the rate of change in magnetic field strength with spatial position.

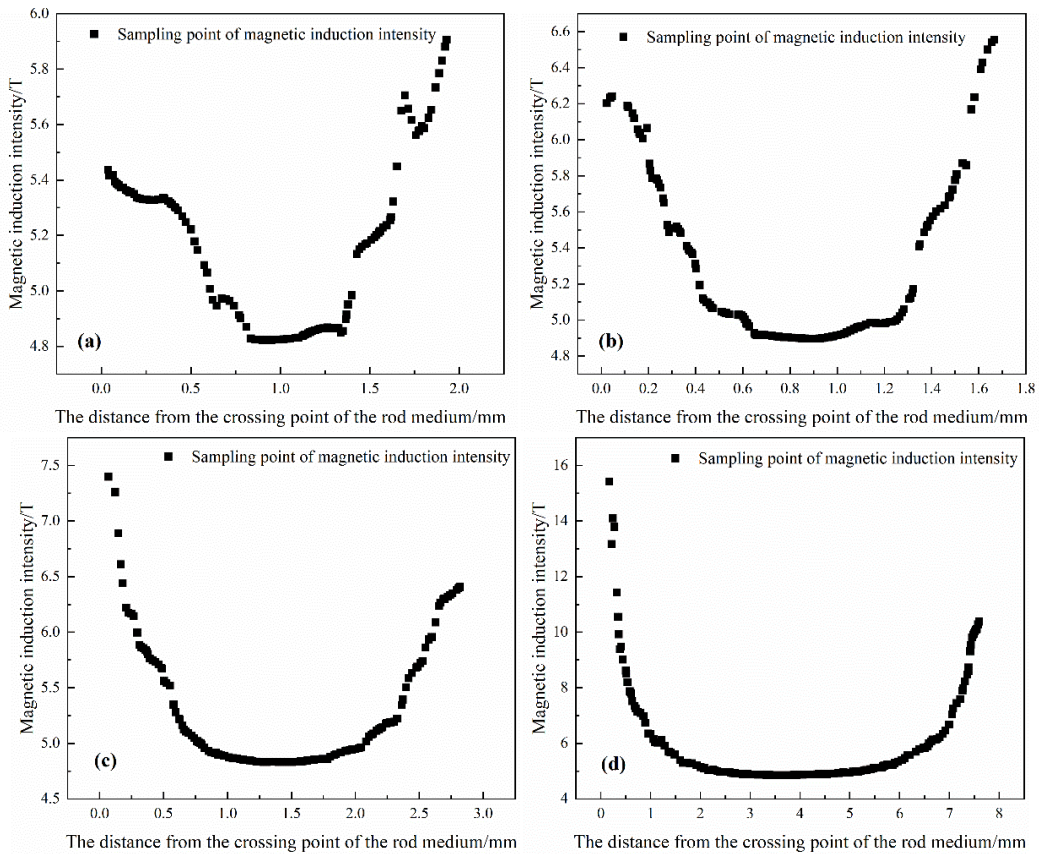


Fig. 17. The magnetic induction intensity on the surface of the polymagnetic matrices varies with distance

Across varying diameters, the longitudinal variation along the XY cross-section exhibits a consistent pattern relative to the rod medium's intersection. The magnetic induction intensity peaks near the contact points with the rod medium and progressively decreases along the longitudinal axis as the distance from these points increases. The magnetic induction intensity reaches its minimum at the midpoint between the two contact points. Analysis reveals that under constant excitation conditions, a decrease in the diameter of the rod medium results in a reduced magnetic induction intensity at the contact points, leading to a more uniform distribution of magnetic induction intensity. This occurs because smaller-diameter magnetic media offer additional pathways for magnetic field lines, thereby decreasing local magnetic resistance. Reduced magnetic resistance facilitates easier distribution of magnetic field lines across the separation area, leading to a decrease in overall magnetic field strength while achieving a more uniform distribution. Smaller diameters generally allow for a higher density of media units within the same space, increasing the number of pathways available for magnetic field lines and thereby reducing the magnetic field strength experienced by each unit of media. Consequently, while the overall magnetic field strength diminishes, the increased number of pathways leads to a more uniform distribution of the magnetic field.

3.3. Discussion

The magnetic field simulation results, encompassing both scenarios with and without magnetic media, provide essential insights into the operational dynamics and optimization strategies for superconducting magnetic separation systems. Simulations conducted without magnetic media establish a baseline for understanding the distribution of the magnetic field within the separation chamber. The observed dumbbell-shaped distribution in the absence of magnetic media reveals that the magnetic field strength is maximal near the coil and diminishes both radially and axially. This gradient is crucial for comprehending how magnetic forces interact with particles during the separation process.

The introduction of magnetic media significantly alters the distribution of the magnetic field. For example, mesh media with smaller gaps yield a more uniform distribution of the magnetic field, which is especially advantageous for the separation of fine particles. This effect is due to the fact that smaller mesh sizes offer more pathways for magnetic field lines, thereby reducing local magnetic resistance and resulting in a more even distribution of the magnetic field. Conversely, larger mesh sizes diminish the focusing effect of the magnetic field, resulting in a less uniform distribution and a more pronounced dumbbell shape.

Rod media similarly affect the magnetic field distribution, with smaller diameter rods generating a denser concentration of magnetic field lines near their surfaces. This increased magnetic field gradient is critical for the effective separation of particles with low magnetic susceptibility. The simulations underscore that rod diameter is a significant factor, with smaller diameters producing a higher magnetic field gradient, thereby enhancing separation efficiency.

The practical implications of these findings are substantial. When designing SMS, the selection of magnetic media should be tailored to the specific requirements of the separation process. For instance, applications necessitating the separation of fine particles or those with low magnetic susceptibility would benefit from media that produce a higher and more uniform magnetic field gradient. This study offers a framework for the selection and optimization of magnetic media, thereby enhancing the performance of superconducting magnetic separators.

However, it is essential to acknowledge the limitations inherent in this study. The simulations were based on idealized models and did not incorporate factors such as material imperfections or fluid dynamics within the separation chamber. These factors could affect the magnetic field distribution and overall separation efficiency in practical applications. Future research should integrate these variables to achieve a more comprehensive understanding of the system's behavior under realistic operational conditions.

Additionally, although this study concentrated on mesh and rod media, investigating other types of magnetic media and their configurations could provide further insights into optimizing magnetic separators. Examining the effects of different media materials, shapes, and arrangements on magnetic field distribution and separation efficiency would be highly beneficial. Moreover, experimental validation of the simulation results would enhance the practical relevance of the findings and aid in

refining the models utilized in this study. Through meticulous selection and configuration of magnetic media, it is feasible to improve separation efficiency and adapt the technology for a broader spectrum of industrial applications. Future research should address the identified limitations and broaden the scope to include additional variables and experimental validations.

4. Conclusions

This study investigates the magnetic field distribution within superconducting magnetic separators, both with and without magnetic media, employing Infolytica MagNet simulations. The primary conclusions are as follows:

1. An analysis of the magnetic induction intensity within the separator's zone was conducted, resulting in the development of a formula that characterizes its distribution and variation in the absence of magnetic media.
2. In the absence of magnetic media, the magnetic field within the separation chamber exhibited a distinctive dumbbell-shaped distribution, characterized by elevated field strengths proximal to the coils and diminished strengths toward the central and end regions.
3. The utilization of smaller mesh media sizes yielded a more uniform magnetic field distribution, whereas larger mesh sizes diminished the magnetic field focusing effect, thereby accentuating the dumbbell shape.
4. Rod media with smaller diameters produced a denser concentration of magnetic field lines near their surfaces, indicative of a higher magnetic field gradient, whereas larger-diameter rods resulted in more pronounced field distortions.
5. These findings underscore the importance of optimizing both the size and configuration of magnetic media to significantly enhance the performance and efficiency of superconducting magnetic separators, thereby facilitating more effective applications in industrial contexts.

Acknowledgments

The authors acknowledge financial support from the National Natural Science Foundation of China (52174243), the Joint Fund (Key program U2067201) for Nuclear Technology Innovation Sponsored by the National Natural Science Foundation of China and the China National Nuclear Corporation, and Nuclear Technology R&D Program.

6. References

- AHORANTA, M., Lehtonen, J., MIKKONEN, R., 2003. *Magnet design for superconducting open gradient magnetic separator*. *Physica C Supercond.*, 386, pp.398-402.
- CAO, S., WEL, D., LI, J., 2019. *Effect of Magnetic Field in Magnetic Separation Column on Particle Separation Process Based on Numerical Simulation*. *J. Eng. Sci. Technol. Rev*, 12(2).
- FUCHINO, S., FURUSE, M., AGATSUMA, K., KAMIOKA, Y., IITSUKA, T., NAKAMURA, S., UEDA, H., KAJIKAWA, K., 2013. *Development of superconducting high gradient magnetic separation system for medical protein separation*. *IEEE T Appl. Supercon.*, 24(3), pp.1-4.
- GILLET, G., DIOT, F., 1999. *Technology of superconducting magnetic separation in mineral and environmental processing*. *Mining Metal Explor.*, 16(3), pp.1-7.
- HU, Z., ZHANG, J., LIU, J., TANG, Y., ZHENG, X., 2020. *Model of particle accumulation on matrices in transverse field pulsating high gradient magnetic separator*. *Miner. Eng.*, 146, p.106105.
- IANNICELLI, J., PECHIN, J., UEYAMA, M., OHKURA, K., HAYASHI, K., SATO, K., LAUDER, A., REY, C., 1997. *Magnetic separation of kaolin clay using a high temperature superconducting magnet system*. *IEEE T Appl. Supercon.*, 7(2), pp.1061-1064.
- IRANMANESH, M., HULLIGER, J., 2017. *Magnetic separation: its application in mining, waste purification, medicine, biochemistry and chemistry*. *Chem. Soc. Rev*, 46(19), pp.5925-5934.
- LI, W., ZHOU, L., HAN, Y., XU, R., 2019. *Numerical simulation and experimental verification for magnetic field analysis of thread magnetic matrix in high gradient magnetic separation*. *Powder Technol.*, 355, pp.300-308.
- LIU, W., ZHENG, C., WU, C., 2022. *Infiltration and resuspension of dilute particle suspensions in micro cavity flow*. *Powder Technol.*, 395,400-411.

- LUO, L., Nguyen, A., 2017. A review of principles and applications of magnetic flocculation to separate ultrafine magnetic particles. *Sep. Purif. Technol*, 172, 85-99.
- MANIOTIS, N., KALAITZIDOU, K., ASIMOULAS, E., SIMEONIDIS, K., 2023. A rotary magnetic separator integrating nanoparticle-assisted water purification: Simulation and laboratory validation. *J. Water Process.*, 53, p.103825.
- NAKAI, Y., MISHIMA, F., AKIYAMA, Y. and NISHIJIMA, S., 2010. Development of high gradient magnetic separation system under dry condition. *Physica C Supercond*, 470(20), pp.1812-1817.
- OHARA, T., KUMAKURA, H., WADA, H., 2001. Magnetic separation using superconducting magnets. *Physica C Supercond*, 357, pp.1272-1280.
- SHARMA, R.G., 2021. *Superconductivity: Basics and applications to magnets (Vol. 214)*. Springer Nature.
- SUPREETH, D.K., BEKINAL, S.I., CHANDRANNA, S.R., DODDAMANI, M., 2022. A review of superconducting magnetic bearings and their application. *IEEE T. Appl. Supercon.*, 32(3), pp.1-15.
- WANG, F., TANG, D., GAO, L., DAI, H., JIANG, P., LU, M., 2020. Dynamic capture and accumulation of multiple types of magnetic particles based on fully coupled multiphysics model in multiwire matrix for high-gradient magnetic separation. *Adv. Powder Technol.*, 31(3), pp.1040-1050.
- WATSON, J.H., BEHARRELL, P.A., 2022. *Magnetic separation*. In *Handbook of Superconductivity* (pp. 572-582). CRC Press.
- WATSON, J. H. P., 1994. Status of superconducting magnetic separation in the minerals industry. *Miner. Eng.*, 7.5-6: 737-746.
- XUE, Z., WANG, Y., ZHENG, X., LU, D., LI, X., 2020. Particle capture of special cross-section matrices in axial high gradient magnetic separation: A 3D simulation. *Sep. Purif. Technol.*, 237, p.116375.
- XU, Z., BO, X., WU, H., TANG, Z., CHEN, F., CHEN, K., WANG, X., ZHANG, G., JIANG, S., 2021. Numerical simulation of contact and separation of magnetic particles under uniform magnetic field. *J Phys. D. Appl. Phys.*, 55(8), p.085001.
- XUE, Z., WANG, Y., ZHENG, X., LU, D., SUN, Z., JING, Z., 2022. Mechanical entrainment study by separately collecting particle deposit on matrix in high gradient magnetic separation. *Miner. Eng.*, 178, p.107435.
- YAMATO, M., KIMURA, T., 2020. Magnetic processing of diamagnetic materials. *Polymers*, 12(7), p.1491.
- ZHENG, X., GUO, N., CUI, R., LU, D., LI, X., LI, M., WANG, Y., 2022. Magnetic field simulation and experimental tests of special cross-sectional shape matrices for high gradient magnetic separation. *IEEE T. Magn.*, 53(3), pp.1-10.
- ZHOU, L., LI, W., HAN, Y., LI, Y., LIU, D., 2021. Numerical simulation for magnetic field analysis and magnetic adsorption behavior of ellipse magnetic matrices in HGMS: Prediction magnetic adsorption behavior via numerical simulation. *Miner. Eng.*, 167, p.106876.